



Cite this: *Chem. Sci.*, 2020, **11**, 2231

All publication charges for this article have been paid for by the Royal Society of Chemistry

Received 11th October 2019
 Accepted 8th January 2020

DOI: 10.1039/c9sc05161a
rsc.li/chemical-science

Introduction

While complex molecular architectures are usually constructed using key bond-making reactions, destructive reactions, in which key bonds are broken, can also be used to advantage. Here we examine the mechanism and consequences of a particular type of molecular destruction – divergent extended heterolytic fragmentation. Carbon–carbon (C–C), carbon–heteroatom (C–X), and heteroatom–heteroatom (X–Y) heterolytic fragmentation reactions offer methods for synthesizing structural motifs (some found in complex natural products) that might be difficult to synthesize using methods focused on bond formation.^{1–7} Despite their continued use in organic synthesis^{8–17} and their relevance to reactions occurring in mass spectrometers,¹⁸ the application of heterolytic fragmentations in which multiple σ -bonds are cleaved in synthetic campaigns is limited by putative strict conformational requirements (*e.g.*, an anti-periplanar conformation for the bonds that cleave during fragmentation; Scheme 1).^{4,19} Few theoretical and mechanistic studies^{20–24} have provided insight into the physical underpinnings for this class of reaction since the seminal work of Grob.² Our aim in this arena is to increase the understanding of underlying mechanistic factors that govern these transformations to facilitate recognition of key patterns associated with fragmentation reactivity and thereby help guide syntheses of compounds whose construction remains a challenge.

Two types of heterolytic fragmentations that have been reported in the literature but have received little theoretical attention are (1) extended fragmentations – heterolytic fragmentations that involve a chain of more than five atoms – and

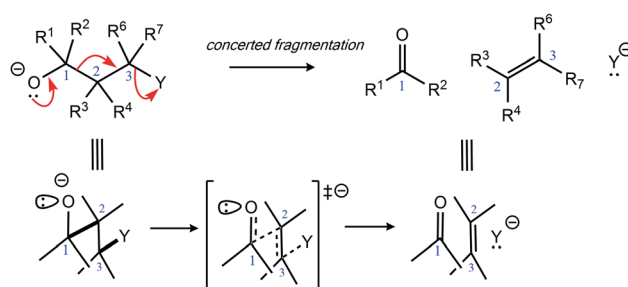
Tipping the balance: theoretical interrogation of divergent extended heterolytic fragmentations†

Croix J. Laconsay, Ka Yi Tsui and Dean J. Tantillo *
 *Correspondence: dtantillo@ucdavis.edu

Herein we interrogate a type of heterolytic fragmentation reaction called a 'divergent fragmentation' using density functional theory (DFT), natural bond orbital (NBO) analysis, *ab initio* molecular dynamics (AIMD), and external electric field (EEF) calculations. We demonstrate that substituents, electrostatic environment and non-statistical dynamic effects all influence product selectivity in reactions that involve divergent fragmentation pathways. Direct dynamics simulations reveal an unexpected post-transition state bifurcation (PTSB), and EEF calculations suggest that some transition states for divergent pathways can, in principle, be selectively stabilized if an electric field of the correct magnitude is oriented appropriately.

(2) divergent fragmentations – heterolytic fragmentations that involve the formation of two (or more) distinct products from a single substrate.⁴ Extended fragmentations are unsurprisingly rare due to the complexity of orchestrating many bond-breaking events in one transformation.²⁵ Some experimental examples are shown in Fig. 1a and b.^{26–28} Highlighted in bold are the bonds involved in each fragmentation. Here we focus on designing systems where these sorts of cage-supported extended fragmentations can have divergent outcomes (Fig. 1d; inspired by reaction in Fig. 1c).

Initially, our objective was to find the length limit for a concerted extended fragmentation, but we encountered unexpected divergent fragmentations en route to this goal; our work on this length limit will be reported elsewhere. Using model systems inspired by experimentally relevant molecules,²⁸ we show that the outcome of divergent fragmentations can be substituent dependent, is sensitive to external electrostatic environments (*i.e.*, in external electric fields (EEFs)), and can involve unusual potential energy surfaces (PESs) with features such as plateaus and post-transition state bifurcations (PTSBs,^{29–34} which make these reactions subject to non-statistical dynamic effects).^{35–38} The particular systems we examine (Fig. 1d and Scheme 2) involve divergence after the first

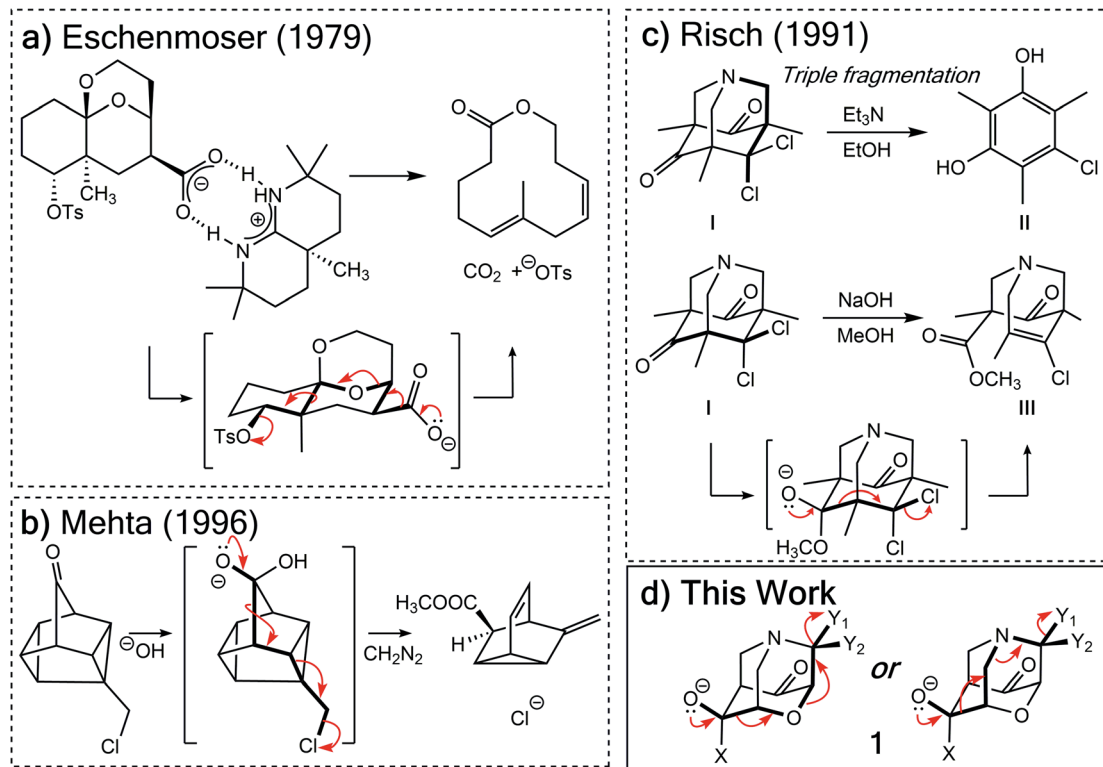


Scheme 1 General heterolytic fragmentation.

Department of Chemistry, University of California, Davis, CA 95616, USA. E-mail: dtantillo@ucdavis.edu

† Electronic supplementary information (ESI) available. See DOI: [10.1039/c9sc05161a](https://doi.org/10.1039/c9sc05161a)



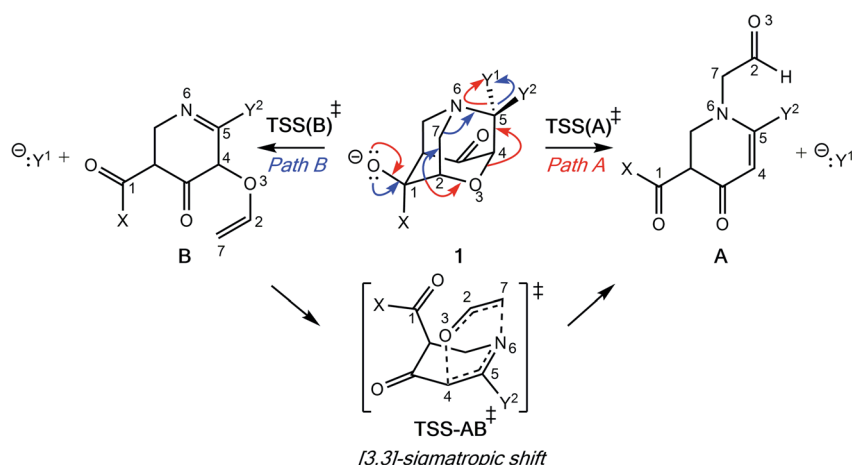
Fig. 1 Previous extended heterolytic fragmentations.^{26–28}

σ -bond has broken, complicating the issue of where along the fragmentation reaction coordinate product selectivity is determined.

Methods

All density functional theory (DFT) calculations were carried out using the Gaussian 09 suite of programs.³⁹ Transition-state structures (TSSs) and minima were verified as such by frequency calculations. Intrinsic Reaction Coordinate (IRC) calculations were used to further characterize TSSs.^{40–42} Eight

different functionals were tested against B3LYP-D3(BJ) for Table 1, entry 1 to verify that geometries of TSSs and minima were reasonably consistent among various methods (see Table S1 in the ESI†). However, the difference in free energy barriers identified by these functionals ranged over more than 10 kcal mol^{−1}. Thus, B3LYP-D3(BJ) and M06-2X, each with the 6-31G(d) basis set, were tested against each other for entries 1–12 in Table 1, since, together, these two functionals covered the range of activation barriers. Employing these two functionals provided a check that DFT reasonably captured the qualitative product selectivity trends with which this study is



Scheme 2 Divergent fragmentation pathways of 1.

Table 1 Substituent effect on divergent fragmentation pathway. Free energy barriers (ΔG^\ddagger) are reported in kcal mol⁻¹

Entry	X	Y ¹	Y ²	$\Delta G_{\text{B3LYP-D3(BJ)}}^\ddagger, \mathbf{A}$	$\Delta G_{\text{M06-2X}}^\ddagger, \mathbf{A}$	$\Delta G_{\text{B3LYP-D3(BJ)}}^\ddagger, \mathbf{B}$	$\Delta G_{\text{M06-2X}}^\ddagger, \mathbf{B}$	Predicted kinetic product(s)
1	N(CH ₃) ₂	O(CO)Cl	H	33.8	46.9	—	—	A
2	N(CH ₃) ₂	Cl	Cl	—	—	32.9	44.1	B
3	NH ₂	O(CO)Cl	H	28.5	39.4	—	—	A
4 ^a	NH ₂	Cl	Cl	28.2	41.5	—	38.8	A & B
5	OCH ₃	O(CO)Cl	H	34.4	46.8	—	—	A
6	OCH ₃	Cl	Cl	—	48.2	33.6	43.8	B
7	OCH(CH ₃) ₂	O(CO)Cl	H	36.7	47.9	—	—	A
8	OCH(CH ₃) ₂	Cl	Cl	37.3	51.1	35.9	47.0	B
9	H	O(CO)Cl	H	35.2	47.5	—	—	A
10	H	Cl	Cl	36.4	49.4	34.6	44.6	B
11	F	O(CO)Cl	H	38.1	50.6	—	—	A
12	F	Cl	Cl	39.2	52.7	37.6	47.7	B

^a The TSS computed at B3LYP-D3(BJ) leads to product **A** only and the TSS computed at M06-2X leads to **B** by an IRC. A TSS that leads to **A** at M06-2X was also identified, but it does not connect to minimum **1** by an IRC.

concerned. Employing a larger basis set (that includes diffuse functions), 6-31+G(d), did not change the overall qualitative conclusions, therefore we only report 6-31G(d) results from here on (see ESI†). Quasi-classical *ab initio* direct dynamics simulations for entries 3 and 4 in Table 1 were initiated from optimized TSSs using the Progdyn script package provided by Singleton.⁴³ Trajectories were propagated in time in both the reactant and product directions until they reached product or reactant wells on the PES: trajectories were allowed to propagate until either the C¹–C² bond (Scheme 2) distance dropped below 1.58 Å, for which we report the trajectory as forming

reactant **1**, until the O³–C⁴ bond distance exceeded 3.2 Å and the C⁵–Y¹ bond distance exceeded 3.0 Å (while C⁵–Y¹ remained below 5.5 Å), for which we report the trajectory as forming product **A**, or until the C⁷–N⁶ bond distance exceeded 3.2 Å and the C⁵–Y¹ bond distance exceeded 3.0 Å (while C⁵–Y¹ remained below 5.5 Å), for which we report the trajectory as forming product **B**. External Electric Field (EEF) calculations⁴⁴ were implemented using the “field” keyword in Gaussian 09 (see ESI† for details).³⁹ A more recent study, in the form of the TITAN code, expands the various types of EEFs that can be generated.⁴⁵

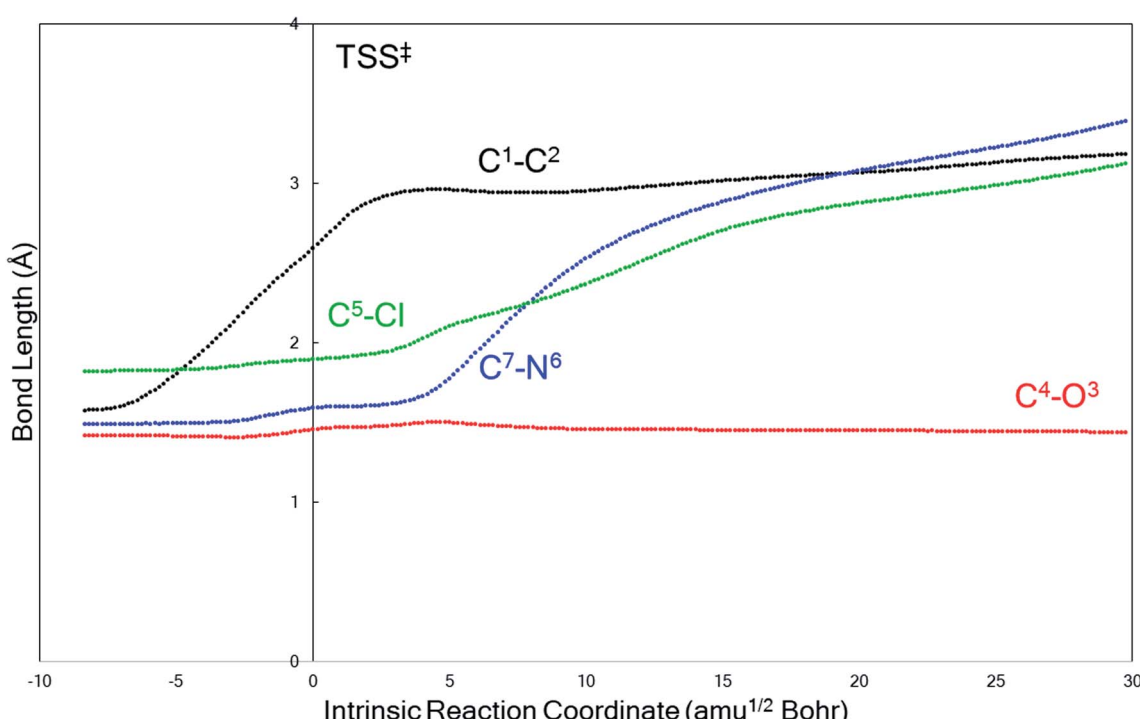


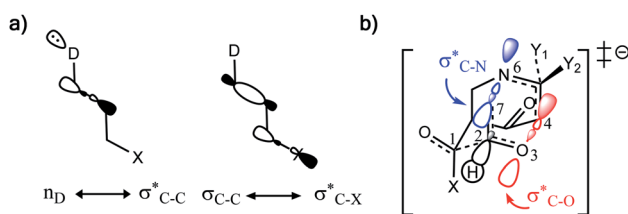
Fig. 2 A representative example (from entry 4 of Table 1, M06-2X/6-31G(d)) of the evolution of key bond lengths involved in the fragmentation as the reaction progresses along the IRC. The transition state structure is at reaction coordinate = 0.



Results and discussion

Substituent effects on product selectivity

In the course of our search for the length limit in concerted fragmentation, we found inspiration in Risch's 1-aza-adamantane (**1** in Fig. 1c).^{28,46} These 1-aza-adamantane structures have played a significant role in work done by the Castellano group in studying donor-acceptor through-bond interactions for crystal and materials design.^{47–49} A simplified model system was designed such that it satisfied the expected structural and stereoelectronic requirements⁵⁰ for concerted fragmentation (**1**, Scheme 2). We hypothesized that this model system would undergo one of two possible concerted 7-atom fragmentations (red and blue arrows in Scheme 2). We successfully found a TSS, **TSS(A)[‡]**, that connects **1** to a product of extended fragmentation (**A**; verified by IRC calculations; see ESI[†]), where $X = \text{OCH}_3$, $Y^1 = \text{Cl}$ and $Y^2 = \text{Cl}$ (red arrows, Scheme 2).



Scheme 3 (a) Double hyperconjugation. (b) The $\sigma_{\text{C}-\text{H}}$ orbital is parallel with respect to antibonding molecular orbitals ($\sigma_{\text{C}-\text{N}}^*$ and $\sigma_{\text{C}-\text{O}}^*$) of **1**.

Table 2 $E(2)$ values corresponding to the magnitude of donor-acceptor interactions involving σ^* orbitals of $\text{C}-\text{O}$ and $\text{C}-\text{N}$ bonds (kcal mol⁻¹; interactions involving all donors are summed)

Entry	$\sigma_{\text{C}_4-\text{O}_3}^*$	$\sigma_{\text{C}_7-\text{N}_6}^*$	Predicted kinetic product(s)
1	80.9	16.5	A
2	16.8	430.3	B
4	21.6	29.8	A & B

Table 3 Wiberg bond order at the TS and bond order change (ΔBO) of the C^4-O^3 and C^7-N^6 bonds that break in forming products **A** and **B**, respectively. Wiberg BOs of reactants are omitted for clarity. Values are computed for M06-2X/6-31G(d) structures. Bold values correspond to products identified by an IRC calculation

Entry	Wiberg BO, reactant ^{C-O}	Wiberg BO, reactant ^{C-N}	Wiberg BO, TSS ^{C-O}	Wiberg BO, TSS ^{C-N}	$\Delta\text{BO}^{\text{C-O}}$	$\Delta\text{BO}^{\text{C-N}}$	Predicted kinetic product(s)
1	0.92	0.95	0.53	0.92	0.39	0.03	A
2	0.92	0.92	0.89	0.48	0.03	0.44	B
3	0.91	0.94	0.55	0.92	0.36	0.02	A
4	0.92	0.93	0.87	0.77	0.05	0.16	A & B
5	0.92	0.94	0.49	0.92	0.43	0.02	A
6	0.93	0.93	0.89	0.44	0.04	0.49	B
7	0.92	0.94	0.48	0.92	0.44	0.02	A
8	0.92	0.93	0.89	0.46	0.03	0.47	B
9	0.91	0.94	0.45	0.93	0.46	0.01	A
10	0.92	0.93	0.88	0.40	0.04	0.53	B
11	0.92	0.93	0.51	0.93	0.41	0.00	A
12	0.92	0.93	0.88	0.37	0.04	0.56	B

2).²⁸ We also postulated that changing Y^1 to chloroformate ($\text{O}(\text{CO})\text{Cl}$) with $Y^2 = \text{H}$ might lead to a TSS that involves a concerted 9-atom fragmentation, given that chloroformate could decarboxylate to form CO_2 and Cl^- , which would break one additional bond ($\text{C}-\text{Cl}$). However, following multiple relaxed potential energy surface scans, candidate TSSs only optimized to **TSS(B)[‡]** (for breaking the C^7-N^6 bond; blue arrows in Scheme 2; verified by IRC calculations; see ESI[†]) instead of **TSS(A)[‡]** (for breaking the O^3-C^4 bond), *i.e.*, **TSS(B)[‡]** connects **1** to **B**.

Calculations at the B3LYP-D3(BJ)/6-31G(d) and M06-2X/6-31G(d) levels reveal that the outcome of this divergent fragmentation (**1** can form **A** or **B**) is dependent on substituents X , Y^1 and Y^2 (Table 1). For example, changing the leaving group (or nucleofuge¹), Y^1 , from chloroformate ($\text{O}(\text{CO})\text{Cl}$) to chlorine (Cl) and $Y^2 = \text{hydrogen (H)}$ to chlorine (Cl) switched the energetically preferred fragmentation pathway from Path A to Path B. Additionally, some entries (entries 4, 6, 8, 10, and 12) in Table 1 have competing pathways, *i.e.* we could identify two TSSs on the PES that either lead to products **A** or **B** (products that are kinetically favored are bolded). Attempts to identify competing TSSs for entries including chloroformate at the Y^1 position (odd numbered entries in Table 1) proved unfruitful, as **TSS(A)[‡]** was the only TSS we could identify. We suspect that different through-space and through-bond electronic effects are the cause of different energetically preferred fragmentation mechanisms—this possibility will be discussed further below.^{51–53} Products **A** and **B** can be interconverted by a [3,3]-sigmatropic shift (**TSS-AB[‡]**), but the TSS for this interconversion consistently lies >30 kcal mol⁻¹ uphill in free energy relative to the less thermodynamically stable product (see ESI[†]). Therefore, the influence of this interconversion on product selectivity is presumably negligible at reasonable experimental temperatures. Products **A** and **B** could be of synthetic utility, although synthesis of **1** presents its own challenges. DFT calculations predicted inconsistent results for entries 3 and 4 (*vide infra*). Worth noting here, too, is the effect of polar solvent on product selectivity: for all entries computed at the M06-2X level in an implicit solvent model (CPCM)^{54,55} of water, no change in



product selectivity was observed; at the B3LYP-D3(BJ) level in the same solvent, entries 2, 6, and 8, switched from **B** to **A** as the predicted kinetic product (see ESI† for additional details). Since results in polar solvent are inconclusive, we focus on gas-phase results from here on.

The behavior of the system in entry 4 proved to be sensitive to the theoretical method used. M06-2X calculations predict that product **B** formation is kinetically preferred over product **A**, which means that the C⁴–O³ bond stays intact while the other key bonds fragment. A representative plot of bond length changes along the reaction coordinate (Fig. 2) reveals that this concerted fragmentation reaction is asynchronous: the C¹–C² bond cleaves before the C⁵–Cl or C⁷–N⁶ bonds.^{56–58} However, a search for TSS(**B**)[‡] at the B3LYP-D3(BJ) level only yielded a TSS

connected to product **A**, TSS(**A**)[‡]; after re-optimizing this TSS(**A**)[‡] at the M06-2X level, we identified a product-**A**-forming TSS that does not directly connect to reactant **1** as a minimum by an IRC. Instead, this TSS(**A**)[‡] connected to an enolate structure that is similar to, but lower in energy than, **1**, *i.e.*, a potential precursor to the reactant. Thus, we do not directly compare barriers for two TSSs at the M06-2X level, but we note that TSS(**A**)[‡] is 2.7 kcal mol^{−1} higher in energy than is TSS(**B**)[‡] if we compare the two TSS's free energies to that of **1**. The peculiarities of the system in entry 4 will be discussed in more detail below.

Stereoelectronic effects

Why do different substituents have such a strong influence on which product is favored? We initially hypothesized that what

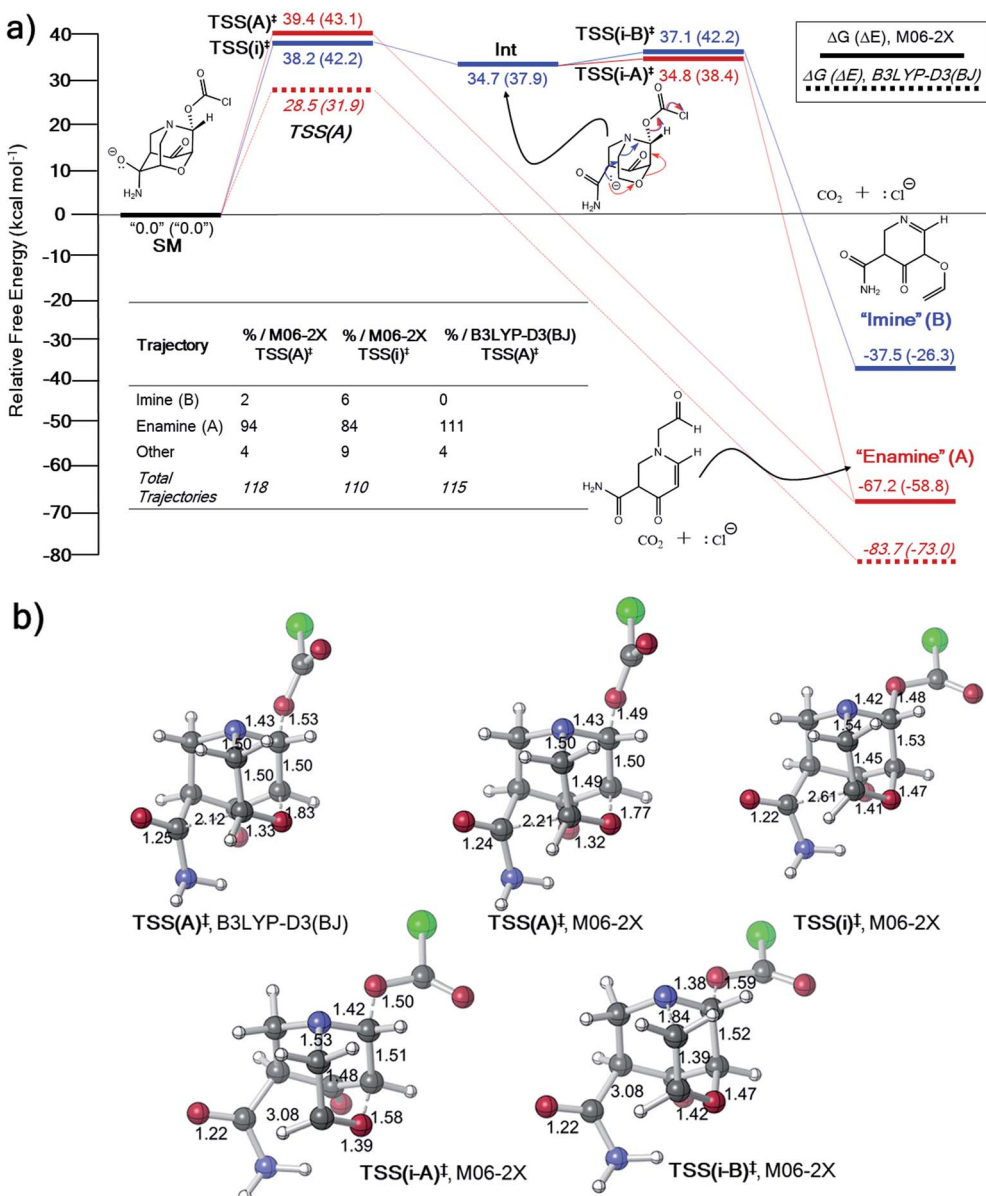


Fig. 3 (a) Free energy profile (electronic energies in parentheses) and “downhill” dynamics results for entry 3 (Table 1). Product distributions from AIMD simulations originate from either TSS(**A**)[‡] or TSS(**i**)[‡]. (b) CYLview images⁷⁸ of key TSSs on the PES for entry 3. Bond lengths in units of Å.



drives the fragmentation towards one product or another is the net sum of stereoelectronic effects within the molecule that would favor breaking either the C⁴–O³ or the N⁶–C⁷ bond. We postulated that the change of one or two substituents would result in a tip in the delicate balance of donor–acceptor interactions and drive reactivity toward one product *versus* the other. Alabugin previously discussed fragmentation reactions in the context of donor–acceptor interactions (see “*Remote Stereoelectronic Effects*”, chapter 8 in ref. 50).⁵⁰ For example, the concept of double hyperconjugation was introduced to explain the extra stabilization (δ -effect) from substituents in δ -cyclohexyl cations.^{59–61} We hypothesized that the geometric restrictions in our 1-aza-adamantane structure would enforce through-bond, ‘double-hyperconjugation-like’ communication through the σ -bond framework. However, in our case, strong double hyperconjugation is not present, since the $\sigma_{C1–C2}$ orbital is not parallel to the $\sigma_{C7–N6}^*$ and $\sigma_{C4–O3}^*$ orbitals (Scheme 3).

To elucidate the key donor–acceptor interactions that might lead to a change in product selectivity, we used NBO calculations, a standard approach for quantifying the magnitude of such interactions.^{50,62,63} A sum of second-order perturbation energies $E(2)$ for TSSs for entries 1, 2 and 4 (Table 1), at the M06-2X/6-31G(d) level, are shown in Table 2 (for the source of these values, see ESI†). The $E(2)$ energies are qualitatively consistent with what is observed in the TSS free energy calculations. For instance, the greater donation of electron density into $\sigma_{C4–O3}^*$ for entry 1 is consistent with formation of product A. The opposite is true for entry 2. Entry 4’s TSS has a similar amount of donation into the σ^* orbitals of both C⁴–O³ and C⁷–N⁶ bonds, which is consistent with different preferred products at different levels of theory (*vide supra*). It is difficult to assign ‘responsibility’ to any one donor–acceptor interaction that favors cleavage of either the C⁴–O³ or C⁷–N⁶ bonds (acceptors), when in fact, it is a multitude of donors that donate electron

density into these σ^* orbitals (see ESI†). One of the major factors contributing to this challenge is the difficulty delineating inductive and field effects in remote stereoelectronic effects.⁵⁰ This is especially prevalent in 1, which as a cage-supported molecule has many through-bond and through-space interactions.

The results above are mirrored by computed Wiberg bond indices, or ‘bond orders’ (BO).^{64,65} Wiberg BOs (computed in an NBO calculation) for the C⁴–O³ or C⁷–N⁶ bonds of the reactants alone are not predictive of which bond will break (all range from 0.91–0.94, with only slightly lower BOs for the bond that breaks; see Table 3), consistent with a “dilution” of delocalization between the O[–] lone pair and the bonds that will break, due to the intermediacy of another σ -bond that must break. We also computed the change in the Wiberg BO, Δ BO, which gives us insight into the perturbation each bond experiences upon reaching the TSS (Table 3). Not surprisingly, for most cases, the product formed can be predicted by which bond has the larger Δ BO (*i.e.*, smaller BO in the fragmentation TSS). For the system in entry 4 (Table 1), the Δ BO values are relatively close, however, precluding a clear prediction (*vide infra*).

Post-transition state bifurcations

The inconsistency between the B3LYP-D3(BJ) and M06-2X results in entries 3 and 4 in Table 1 prompted us to explore the potential energy surfaces for these two systems using *ab initio* molecular dynamics (AIMD) simulations.^{33,66–68} Previous work suggests that IRCs obtained with two different theoretical methods that lead to different products despite originating at ostensibly the same TSS could indicate that a PTSB follows this TSS.^{69–71} In all dynamics simulations, trajectories were initiated from the DFT-optimized TSSs and propagated in reactant and product directions until structures were reached that closely

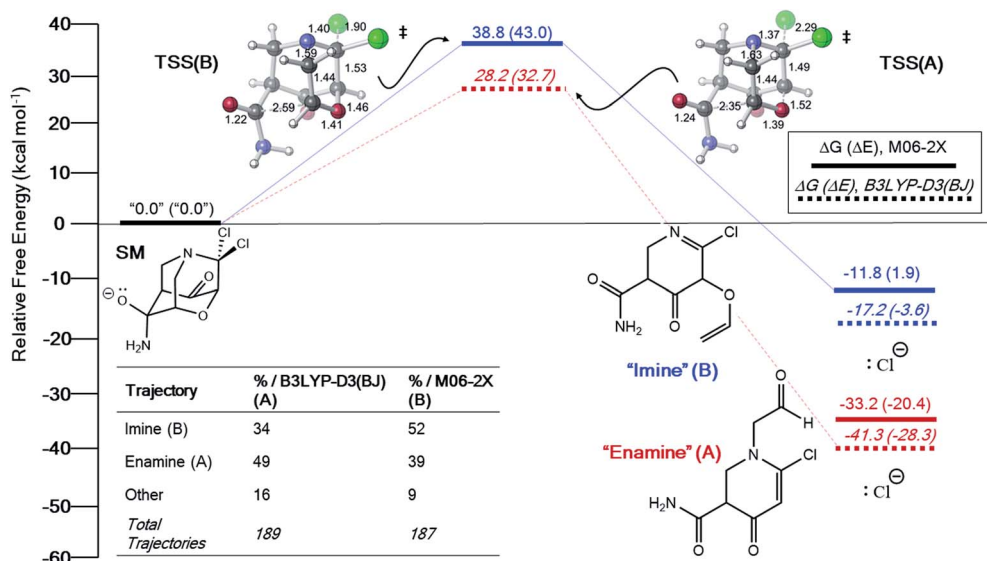


Fig. 4 Free energy profile (electronic energies in parentheses) and “downhill” dynamics results from B3LYP-D3(BJ) and M06-2X PES’s for entry 4 (Table 1). Products that are connected by a solid or dotted line to the TSS indicate that they are connected by an IRC to the reactant.



resembled minima on the PES (see Methods section for details).^{31,33,72-74}

For the system in entry 3 (Table 1), downhill trajectories from **TSS(A)[‡]** predominantly form **A**, with a small number forming **B** (Fig. 3) at the M06-2X level. Product **A** can also originate from a shallow carbanion intermediate, **Int**, formed *via* **TSS(i)[‡]**. **Int** is not found on the B3LYP-D3(BJ) PES (see ESI[†] for IRC).^{75,76} Mandal and Datta reported a similarly shaped PES in a gold(i)-catalyzed Diels–Alder reaction with a single intermediate well leading to two different products where the product selectivity is steered by dynamic effects.⁷⁷ Trajectories originating from **TSS(i)[‡]** also predominantly form **A**, with a slightly larger number

forming **B**. Product **A** is thermodynamically favored, which may manifest in lower energy exit channels from both TSSs on the relatively flat energy surface in the vicinity of **TSS(i-A)[‡]**, **Int** and **TSS(i)[‡]**. No downhill trajectories from **TSS(A)[‡]** result in formation of the imine product (**B**) when using B3LYP-D3(BJ) (Fig. 3a). While the formation of some product **B** is consistent with the presence of a PTSB, the product distribution for this system is probably better described as arising from molecular motion on a flat energy surface.

For the system in entry 4, no intermediate was found at either level of theory (Fig. 4). Again, product **A** is much more favorable in free energy than product **B**. However, our AIMD

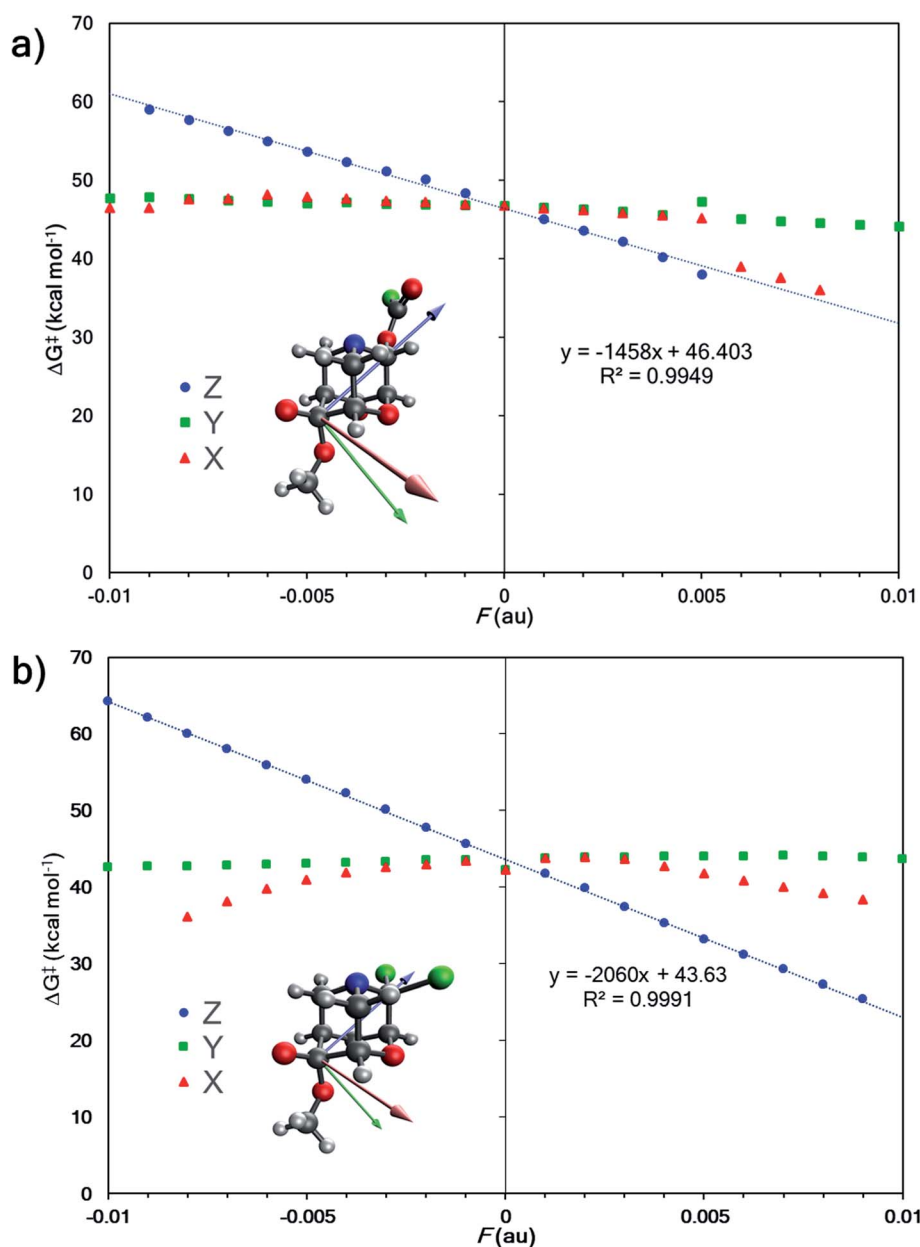


Fig. 5 (a) External electric field effects on divergent fragmentation of **1** (entry 5, TSS for formation of **A** from Table 1). The high green data point at $F_y = +0.005$ results from a change in the reactant structure geometry in the presence of an EEF. Reactant structures optimized in EEFs of $F_y \geq 0.005$ au result in a structure shown in Fig. S3 in ESI.[†] (b) Effects on divergent fragmentation of **1** (entry 6, TSS for formation of **B** from Table 1).



calculations predict that products **A** and **B** are produced in comparable amounts using either functional. These results are consistent with a PTSB on the PES and non-statistical dynamic control of the product distribution.³¹

External electric fields

Since changing substituents X, Y¹, and Y² altered the outcome of divergent fragmentations of **1**, we questioned what might happen under the influence of an external perturbation like an external electric field (EEF). EEFs have recently received considerable attention, being referred to as “smart reagents” for catalysis because of their ability to control reactivity and selectivity.^{44,79–81} A seminal study by Shaik and co-workers demonstrated that not only can an EEF lower or raise the barrier for a Diels–Alder reaction when oriented in one direction or the other along the “reaction axis”—that is, the (approximate) axis

along which electrons reorganize (on average) to make and break bonds—but an electric field oriented perpendicular to the reaction axis can induce endo/exo selectivity.⁸² The potential for EEFs to control chemical transformations has captured the curiosity of many groups^{83–92} since Coote and co-workers experimentally demonstrated electrostatic catalysis of a Diels–Alder reaction in 2016.⁹³ For example, a recent experimental study demonstrated EEF-induced selective catalysis in a two-step reaction.⁹⁴

Effects on reaction rate. Do electric fields oriented in different directions have accelerating/decelerating effects on the rate of fragmentation of **1**? We selected entries 5 and 6 (Table 1) for our case studies because these entries are structurally similar, except for the identity of Y¹ and Y². To start any EEF study, the field’s orientation must be carefully defined (see ESI†).⁴⁴ Fig. 5 depicts the axis orientations employed here for EEF calculations and the effect of varying EEFs on the free energy barrier (see Fig. S6 and S9 in the ESI† for representative examples of similar results with different axis orientations). These results indicate that orienting the electric field down the “reaction-axis” (z) leads to an approximately linear change in activation barrier, which is consistent with what is known so far of EEF effects on reactivity.⁴⁴ Orienting an electric field in other directions has a weaker effect, as expected.⁹³

Effects on product selectivity—divergent outcomes from a single reactant. How is product selectivity impacted in divergent heterolytic fragmentations in the presence of an EEF? To test this idea, we turned to a previous study that examined a simpler divergent fragmentation using both experiment and theory. While examining a C–C bond fragmentation approach to synthesize allenes (Fig. 6), Williams and co-workers observed that both alkyne and allene products were formed initially, in a $>20 : 1$ ratio.⁹⁵ Over time, they observed that this ratio decreased to 3 : 1 favoring the allene. Our computed enthalpies and free energies agree qualitatively with their reported

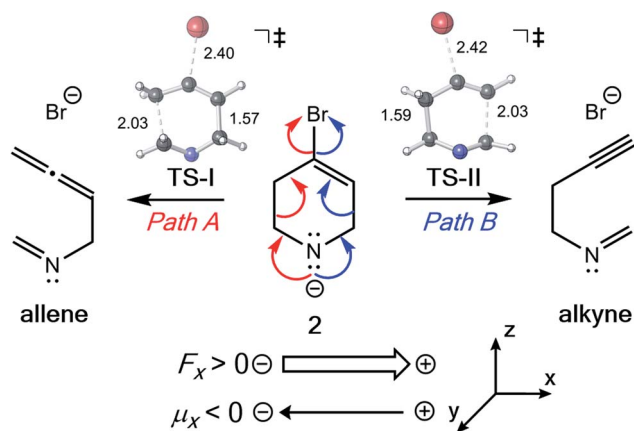


Fig. 6 Fragmentation reaction of Williams and co-workers examined in the presence of EEFs. M06-2X/6-31G(d) optimized TS-I and TS-II are shown with key bond lengths in Å.

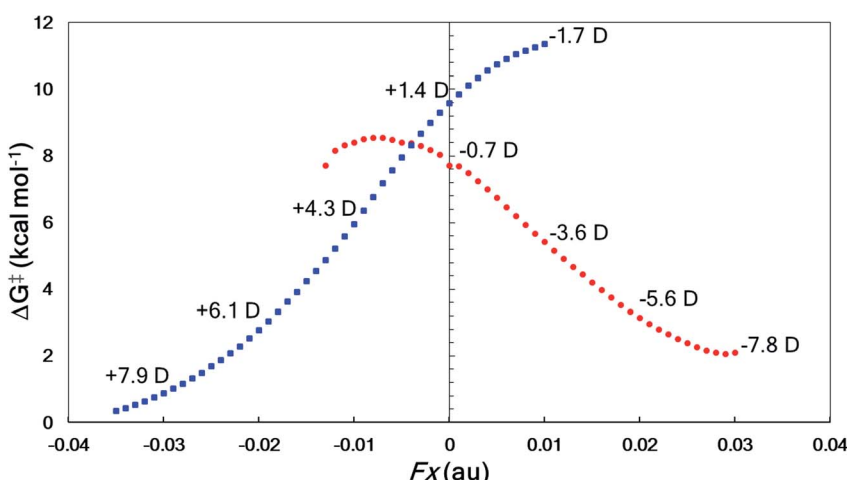


Fig. 7 EEF effects on divergent fragmentation of **2**, examined using M06-2X/6-31G(d). The x component of the molecular dipole moment (μ_x in Debye) is shown at each hundredth of an atomic unit (au) representing the magnitude of the electric field oriented in the $\pm x$ direction. Red circles correspond to Path A in Fig. 6 and blue squares correspond to Path B. At points where the trendline falls off, we find that either the reactant structure and/or the TSS are not stationary points on the PES.



computational results and are consistent with experimental observations that initial allene formation is faster than alkyne formation: the predicted $\Delta\Delta G^\ddagger$ between **TS-II** and **TS-I** is 2.6 kcal mol⁻¹ with B3LYP-D3(BJ) and 1.9 kcal mol⁻¹ with M06-2X (see Table S5† for details). We envisioned that, since EEFs have a rate accelerating/decelerating effect, they also may have the ability to induce product selectivity in divergent fragmentations.

The directional flow of electrons (reaction axis⁴⁴) in this system is assumed to point from the N atom to the Br atom down the $+z$ axis (Fig. 6). We postulated that, perpendicular to that axis, along the $\pm x$ axis, electron flow would be polarized so as to favor either Path A or Path B, *i.e.*, one of **TS-I** and **TS-II** would be selectively stabilized while the other would be

destabilized. This prediction is borne out in our computations (Fig. 7). With a field of magnitude 0.004 au oriented in the $-x$ direction, the free energy barriers for formation of the allene and alkyne are predicted to be equal, but different products are favored at higher or lower field strengths, *i.e.*, there exists a mechanistic crossover point somewhere along the EEF spectrum. While the crossover point might occur at a different field strength with a different level of theory, this example serves as a proof-of-concept that one might be able to selectively produce either product of a divergent fragmentation with an appropriately oriented electric field.

Do EEF's have a similar effect on product selectivity in the fragmentation of **1**? To answer this question, we selected entries 6 and 10 (from Table 1) for our case studies because these entries

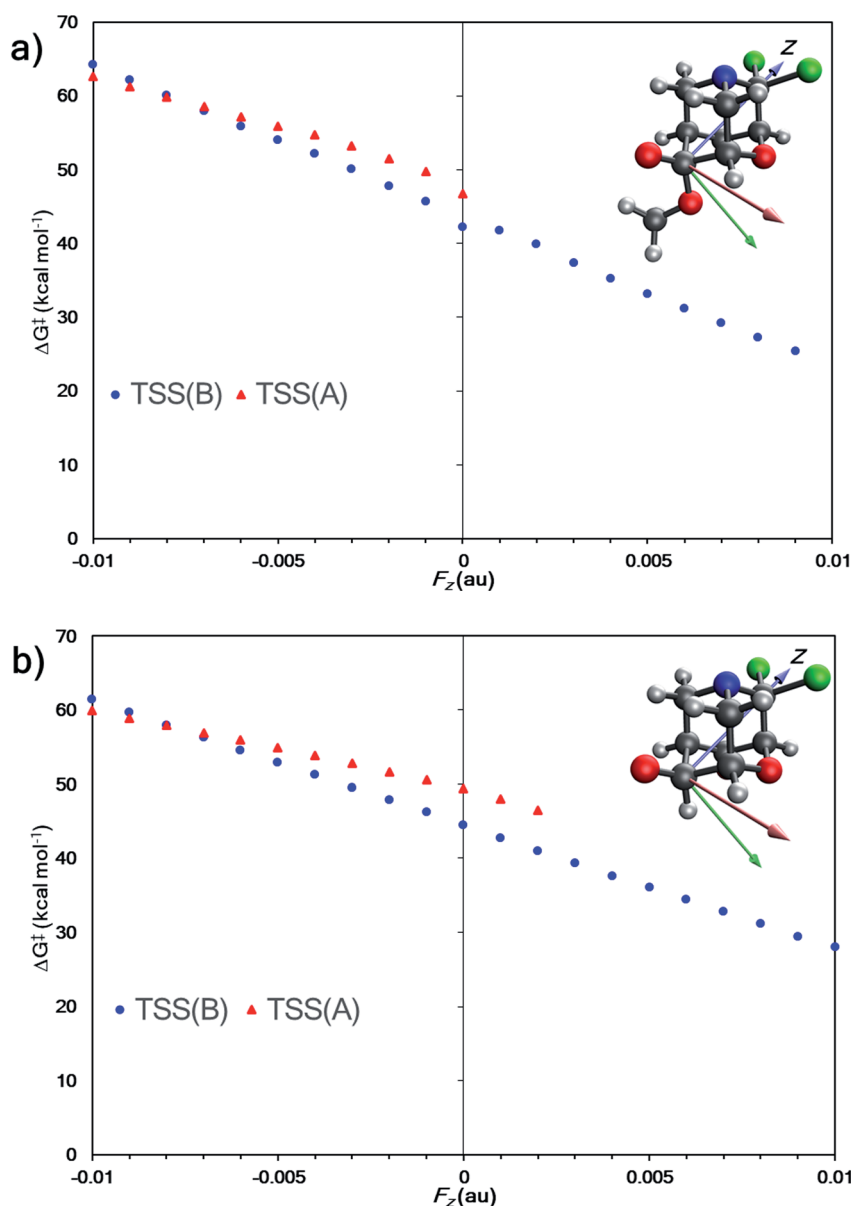


Fig. 8 (a) External electric field effects ($\pm F_z$) on divergent fragmentation of **1** (entry 6, TSSs for formation of A and B from Table 1). (b) Effects on divergent fragmentation of **1** (entry 10, TSSs for formation of A and B from Table 1).



each have two TSSs—one leading to product **A** (**TSS(A)**[‡]) and one leading to product **B** (**TSS(B)**[‡]). In both cases, product **B** is kinetically preferred in the absence of an EEF (with both B3LYP-D3(BJ) and M06-2X). The results of the EEF calculations in Fig. 5 indicate that the *z* axis induces the most significant change to the free energy barrier. We hypothesized that an EEF along the $\pm z$ axis might have a significant (de)stabilizing effect on the free energy barriers, enough to switch product selectivity. Fig. 8 displays the results of the calculations. Both **TSS(A)**[‡] and **TSS(B)**[‡] experience a linear change in the free energy barrier. However, only the barrier for formation of **B** is lowered in the presence of positive *z* ($+F_z$) fields: attempts to optimize **TSS(A)**[‡] in the presence of EEFs of $+F_z > 0.001$ au for entry 6 and $+F_z > 0.003$ for entry 10 led to **TSS(B)**[‡]. This suggests that fields oriented in that direction might completely shut down the pathway to form product **A**. We also carried out calculations in which an EEF is oriented along the $\pm x$ or $\pm y$ axes, to test for switches in product selectivity (see ESI, Fig. S7 and S8†), but observed no crossing of the free energy barriers for **TSS(A)**[‡] and **TSS(B)**[‡]. This means that there is no switch in selectivity for the divergent fragmentation of **1** in the presence of EEFs oriented in the *x* or *y* directions within the -0.01 au to $+0.01$ au magnitude range.⁹⁵ Nevertheless, as EEFs in the $-F_z$ direction increase in magnitude, the $\Delta\Delta G^\ddagger$ between **TSS(A)**[‡] and **TSS(B)**[‡] decreases (making the path to form **A** more competitive), and at some field, the selectivity switches. This, in principle, means that EEFs oriented down the $\pm z$ axis can alter product selectivity.

Conclusions

Since the 1950s, with the identification and categorization of fragmentations as a class of organic reaction by Eschenmoser⁹⁶ and its further development by Grob (with “...glaring disregard of the earlier contributions”³),^{1,2} the heterolytic fragmentation has become a useful tool in organic synthesis. Nonetheless, we believe that additional interesting chemistry remains to be discovered in this area. In this study, we have expanded the concept of heterolytic fragmentation by exploring a model fragmentation in which a single substrate can fragment *via* two distinct pathways to different products after an initial σ -bond cleavage – a divergent extended fragmentation.⁴ We demonstrated that substituents, electrostatic environment and dynamic effects can influence pathways to competing products. Direct dynamics simulations on some systems reveal flat regions of energy surfaces where selectivity is determined and yet another unexpected PTSB in a reaction of a complex organic molecule.³³ Finally, EEF calculations suggest that divergent pathways can, in principle, be selected between if an electric field is oriented appropriately.⁹⁷

Conflicts of interest

There are no conflicts to declare.

Acknowledgements

This work was inspired in part by a friendly competition between the groups of DJT and Roald Hoffmann (Cornell) to

find the limit for combining substitution events into concerted processes. Financial and computational (XSEDE) support from NSF is gratefully acknowledged.

References

- 1 C. A. Grob and P. W. Schiess, *Angew. Chem., Int. Ed.*, 1967, **6**, 1–106.
- 2 C. A. Grob, *Angew. Chem., Int. Ed.*, 1969, **8**, 535–622.
- 3 K. Prantz and J. Mulzer, *Chem. Rev.*, 2010, **110**, 3741–3766.
- 4 M. A. Drahla, M. Manpadi and L. J. Williams, *Angew. Chem., Int. Ed.*, 2013, **52**, 11222–11251.
- 5 P. Weyerstahl and H. Marschall, in *Comprehensive Organic Synthesis*, 1991, pp. 1041–1070.
- 6 T. T. Hoang, G. B. Dudley and L. J. Williams, *Comprehensive Organic Synthesis*, Elsevier Ltd., 2nd edn, 2014, vol. 6, pp. 842–860.
- 7 J. Yang, T. T. Hoang and G. B. Dudley, *Org. Chem. Front.*, 2019, **6**, 2560–2569.
- 8 E. J. Corey, R. B. Mitra and H. Uda, *J. Am. Chem. Soc.*, 1963, **85**, 362–363.
- 9 E. J. Corey, R. B. Mitra and H. Uda, *J. Am. Chem. Soc.*, 1964, **86**, 485–492.
- 10 T. T. Hoang, M. Birepinte, N. M. Kramer and G. B. Dudley, *Org. Lett.*, 2016, **18**, 3470–3473.
- 11 M. M. Uteuliyyev, T. T. Nguyen and D. M. Coltart, *Nat. Chem.*, 2015, **7**, 1024–1027.
- 12 J. Shi, H. Xu, D. Qiu, J. He and Y. Li, *J. Am. Chem. Soc.*, 2016, **139**, 623–626.
- 13 E. J. Rastelli, A. A. Bolinger and D. M. Coltart, *Chem.*, 2018, **4**, 2228–2238.
- 14 J. R. Donald and W. P. Unsworth, *Chem. – Eur. J.*, 2017, **23**, 8780–8799.
- 15 L. Cao, C. Wang and P. Wipf, *Org. Lett.*, 2019, **21**, 1538–1541.
- 16 B. Ma, Y. Zhao, C. He and H. Ding, *Angew. Chem., Int. Ed.*, 2018, **57**, 15567–15571.
- 17 Q. Gu, X. Wang, B. Sun and G. Lin, *Org. Lett.*, 2019, **21**, 5082–5085.
- 18 D. P. Demarque, A. E. M. Crotti, R. Vessecchi, J. L. C. Lopes and N. P. Lopes, *Nat. Prod. Rep.*, 2016, **33**, 432–455.
- 19 R. M. Wilson and S. J. Danishefsky, *J. Org. Chem.*, 2007, **72**, 4293–4305.
- 20 R. L. Davis, C. A. Leverett, D. Romo and D. J. Tantillo, *J. Org. Chem.*, 2011, **76**, 7167–7174.
- 21 J. Andrés, J. J. Queralt, V. S. Safont, M. Canle L and J. A. Santabarria, *J. Phys. Chem.*, 1996, **100**, 3561–3568.
- 22 J. J. Queralt, V. S. Safont, V. Moliner and J. Andrés, *Chem. Phys.*, 1998, **229**, 125–136.
- 23 L. M. LeBlanc, S. W. Powers, J. S. Grossert and R. L. White, *Rapid Commun. Mass Spectrom.*, 2016, **30**, 2133–2144.
- 24 P. Batsomboon, B. A. Gold, I. V. Alabugin and G. B. Dudley, *Synth.*, 2012, **44**, 1818–1824.
- 25 M. Castiñeira Reis, C. S. López, O. Nieto Faza and D. J. Tantillo, *Chem. Sci.*, 2019, **10**, 2159–2170.
- 26 G. Mehta and C. Ravikrishna, *Tetrahedron Lett.*, 1996, **37**, 2655–2658.



27 D. Sternbach, M. Shibuya, F. Jaisli, M. Bonetti and A. Eschenmoser, *Angew. Chem., Int. Ed.*, 1979, **18**, 634–636.

28 N. Risch, M. Langhals and T. Hohberg, *Tetrahedron Lett.*, 1991, **32**, 4465–4468.

29 D. H. Ess, S. E. Wheeler, R. G. Iafe, L. Xu, N. Çelebi-Ölçüm and K. N. Houk, *Angew. Chem., Int. Ed.*, 2008, **47**, 7592–7601.

30 J. Rehbein and B. K. Carpenter, *Phys. Chem. Chem. Phys.*, 2011, **13**, 20906–20922.

31 S. R. Hare and D. J. Tantillo, *Beilstein J. Org. Chem.*, 2016, **12**, 377–390.

32 S. R. Hare and D. J. Tantillo, *Pure Appl. Chem.*, 2017, **89**, 679–698.

33 Z. Yang and K. N. Houk, *Chem. – Eur. J.*, 2018, **24**, 3916–3924.

34 N. Mandal and A. Datta, *J. Phys. Chem. B*, 2018, **122**, 1239–1244.

35 B. K. Carpenter, *Angew. Chem., Int. Ed.*, 1998, **37**, 3340–3350.

36 P. Collins, B. Carpenter, G. Ezra and S. Wiggins, *J. Chem. Phys.*, 2013, **139**, 154108.

37 B. K. Carpenter, *Chem. Rev.*, 2013, **113**, 7265–7286.

38 D. J. Tantillo, *Dynamic Effects on Organic Reactions in Reference Modules in Chemistry, Molecular Sciences and Chemical Engineering*, Elsevier Inc., Waltham, MA, 2018.

39 M. J. Frisch, G. W. Trucks, H. B. Schlegel, B. Scuseria, G. E. Robb, J. R. Cheeseman, G. Scalmani, V. Barone, H. P. Mennucci, G. A. Petersson, H. Nakatsuji, M. Caricato, X. Li, M. Hratchian, A. F. Izmaylov, J. Bloino, G. Zheng, J. L. Sonnenberg, T. Hada, M. Ehara, K. Toyota, R. Fukuda, J. Hasegawa, M. Ishida, J. A. Nakajima, P. Honda, Y. Kitao, O. Nakai, H. Vreven, T. Montgomery, Jr., F. Ogliaro, M. Bearpark, J. J. Heyd, E. Brothers, V. N. Staroverov, V. N. Keith, T. Kobayashi, R. Normand, J. C. K. Rendell, A. Burant, J. C. Iyengar, S. S. Tomasi, J. B. M. Rega, N. Millam, J. M. Klene, M. Knox, J. E. Cross, R. E. Y. Bakken, V. Adamo, C. Jaramillo, J. Gomperts, R. Stratmann, M. O. Austin, R. Cammi, C. Pomelli, R. L. J. W. Ochterski, K. Morokuma, V. G. Zakrzewski, G. A. Voth, P. Salvador, J. J. Dannenberg, S. Dapprich, A. D. Daniels, D. J. O. Foresman, J. B. Ortiz, J. V. Ciosowski and J. Fox, Gaussian Inc., 2009.

40 K. Fukui, *Acc. Chem. Res.*, 1981, **14**, 363–368.

41 C. Gonzalez and H. B. Schlegel, *J. Phys. Chem.*, 1990, **94**, 5523.

42 S. Maeda, Y. Harabuchi, Y. Ono, T. Taketsugu and K. Morokuma, *Int. J. Quantum Chem.*, 2015, **115**, 258–269.

43 D. A. Singleton, C. Hang, M. J. Szymanski and E. E. Greenwald, *J. Am. Chem. Soc.*, 2003, **125**, 1176–1177.

44 S. Shaik, R. Ramanan, D. Danovich and D. Mandal, *Chem. Soc. Rev.*, 2018, **47**, 5125–5145.

45 T. Stuyver, J. Huang, D. Mallick, D. Danovich and S. Shaik, *J. Comput. Chem.*, 2020, **41**, 74–82.

46 D. Kardel, W. Knoche and N. Risch, *J. Chem. Soc., Perkin Trans. 1*, 1993, **2**, 1455–1459.

47 A. J. Lampkins, Y. Li, A. Al Abbas, K. A. Abboud, I. Ghiviriga and R. K. Castellano, *Chem. – Eur. J.*, 2008, **14**, 1452–1463.

48 H. Li, E. A. Homan, A. J. Lampkins, I. Ghiviriga and R. K. Castellano, *Org. Lett.*, 2005, **7**, 443–446.

49 L. Yuan, B. G. Sumpter, K. A. Abboud and R. K. Castellano, *New J. Chem.*, 2008, **32**, 1924–1934.

50 I. V. Alabugin, *Stereoelectronic Effects Stereoelectronic Effects A Bridge Between Structure and Reactivity*, John Wiley & Sons, Ltd, 2016.

51 R. Hoffmann, *Acc. Chem. Res.*, 1971, **4**, 1–9.

52 R. Gleiter, *Angew. Chem., Int. Ed.*, 1974, **13**, 696–701.

53 M. N. Paddon-Row, *Acc. Chem. Res.*, 1982, **15**, 245.

54 V. Barone and M. Cossi, *J. Phys. Chem. A*, 1998, **102**, 1995–2001.

55 M. Cossi, N. Rega, G. Scalmani and V. Barone, *J. Comput. Chem.*, 2003, **24**, 669–681.

56 D. J. Tantillo and J. Tantillo, *J. Phys. Org. Chem.*, 2008, **21**, 561–570.

57 A. Williams, *Concerted Organic and Bioorganic Mechanisms*, CRC Press LLC, 1st edn, 2000.

58 M. J. S. Dewar and A. B. Pierini, *J. Am. Chem. Soc.*, 1984, **106**, 203–208.

59 W. Adcock, J. Cope, V. J. Shiner, Jr. and N. A. Trout, *J. Org. Chem.*, 1990, **55**, 1411–1414.

60 J. B. Lambert, L. A. Salvador and J. H. So, *Organometallics*, 2005, **12**, 697–703.

61 I. V. Alabugin and M. Manoharan, *J. Org. Chem.*, 2004, **69**, 9011–9024.

62 E. D. Glendening, C. R. Landis and F. Weinhold, *J. Comput. Chem.*, 2013, **34**, 1429–1437.

63 F. Weinhold, C. R. Landis and E. D. Glendening, *Int. Rev. Phys. Chem.*, 2016, **35**, 399–440.

64 K. B. Wiberg, *Tetrahedron*, 1968, **24**, 1083–1096.

65 D. E. Ortega, S. Gutiérrez-Oliva, D. J. Tantillo and A. Toral-Blabé, *Phys. Chem. Chem. Phys.*, 2015, **17**, 9771–9779.

66 S. Pratihar, X. Ma, Z. Homayoon, G. L. Barnes and W. L. Hase, *J. Am. Chem. Soc.*, 2017, **139**, 3570–3590.

67 X. Ma and W. L. Hase, *Philos. Trans. R. Soc., A*, 2017, **375**, 20160204.

68 M. Paranjathy, R. Sun, Y. Zhuang and W. L. Hase, *Wiley Interdiscip. Rev.: Comput. Mol. Sci.*, 2013, **3**, 296–316.

69 S. R. Hare and D. J. Tantillo, *Chem. Sci.*, 2017, **8**, 1442–1449.

70 D. H. Nouri and D. J. Tantillo, *J. Org. Chem.*, 2006, **71**, 3686–3695.

71 Y. J. Hong and D. J. Tantillo, *Nat. Chem.*, 2014, **6**, 104–111.

72 U. Lourderaj, K. Park and W. L. Hase, *Int. Rev. Phys. Chem.*, 2008, **27**, 361–403.

73 B. K. Carpenter, *Annu. Rev. Phys. Chem.*, 2005, **56**, 57–89.

74 U. Lourderaj and W. L. Hase, *J. Phys. Chem. A*, 2009, **113**, 2236–2253.

75 M. D. Wodrich, C. Corminboeuf and P. V. R. Schleyer, *Org. Lett.*, 2006, **8**, 3631–3634.

76 V. N. Staroverov and E. R. Davidson, *J. Am. Chem. Soc.*, 2000, **122**, 7377–7385.

77 N. Mandal and A. Datta, *J. Org. Chem.*, 2018, **83**, 11167–11177.

78 C. Y. Legault, *CYLview, 1.0b*, Univ. Sherbrooke, 2009.

79 S. Shaik, D. Mandal and R. Ramanan, *Nat. Chem.*, 2016, **8**, 1–25.

80 S. Ciampi, N. Darwish, H. M. Aitken, I. Díez-Perez and M. L. Coote, *Chem. Soc. Rev.*, 2018, **47**, 5146–5164.



81 T. Stuyver, D. Danovich, J. Joy and S. Shaik, *Wiley Interdiscip. Rev.: Comput. Mol. Sci.*, 2020, e1438.

82 R. Meir, H. Chen, W. Lai and S. Shaik, *ChemPhysChem*, 2010, **11**, 301–310.

83 M. Akamatsu, N. Sakai and S. Matile, *J. Am. Chem. Soc.*, 2017, **139**, 6558–6561.

84 K. Bhattacharyya, S. Karmakar and A. Datta, *Phys. Chem. Chem. Phys.*, 2017, **19**, 22482–22486.

85 W. M. Sun, C. Y. Li, J. Kang, D. Wu, Y. Li, B. L. Ni, X. H. Li and Z. R. Li, *J. Phys. Chem. C*, 2018, **122**, 7867–7876.

86 T. Dudev, S. Ilieva and L. Doudeva, *Phys. Chem. Chem. Phys.*, 2018, **20**, 24633–24640.

87 L. Yue, N. Wang, S. Zhou, X. Sun, M. Schlangen and H. Schwarz, *Angew. Chem., Int. Ed.*, 2018, **57**, 14635–14639.

88 A. A. Arabi and C. F. Matta, *J. Phys. Chem. B*, 2018, **122**, 8631–8641.

89 Z. Wang, D. Danovich, R. Ramanan and S. Shaik, *J. Am. Chem. Soc.*, 2018, **140**, 13350–13359.

90 Y. Zang, Q. Zou, T. Fu, F. Ng, B. Fowler, J. Yang, H. Li, M. L. Steigerwald, C. Nuckolls and L. Venkataraman, *Nat. Commun.*, 2019, **10**, 1–7.

91 C. Geng, J. Li, T. Weiske, M. Schlangen, S. Shaik and H. Schwarz, *J. Am. Chem. Soc.*, 2017, **139**, 1684–1689.

92 A. C. Aragonès, N. L. Haworth, N. Darwish, S. Ciampi, N. J. Bloomfield, G. G. Wallace, I. Diez-Perez and M. L. Coote, *Nature*, 2016, **531**, 88–91.

93 X. Huang, C. Tang, J. Li, L.-C. Chen, J. Zheng, P. Zhang, J. Le, R. Li, X. Li, J. Liu, Y. Yang, J. Shi, Z. Chen, M. Bai, H.-L. Zhang, H. Xia, J. Cheng, Z.-Q. Tian and W. Hong, *Sci. Adv.*, 2019, **5**, eaaw3072.

94 R. V. Kolakowski, M. Manpadi, Y. Zhang, T. J. Emge and L. J. Williams, *J. Am. Chem. Soc.*, 2009, **131**, 12910–12911.

95 Perhaps product selectivity switches at greater magnitudes or under the influence of EEFs oriented in other directions.

96 A. Eschenmoser and A. Frey, *Helv. Chim. Acta*, 1952, **35**, 1660–1666.

97 Altogether, these EEF results may have implications for fragmentation reactions that occur in a variety of environments, for example, in the active sites of enzymes or in solvent in a synthetic laboratory. It is important to recognize that our EEF analysis suffers from some limitations: (1) electric fields are not always homogenous EEFs, (for example in enzymes) and (2) gas-phase quantum calculations can only elucidate EEF effects on static electronic structure and energies of stationary points on our potential energy surface. Perhaps in solution, other significant effects, such as solvent effects, might induce other phenomena that cannot be modeled here. Solvent-solute dynamic effects modeled by explicit solvent were not considered in this study, but it has been discussed recently that local electric field effects due to explicit solvent molecules can alter the PES of the Claisen rearrangement of *cis*-2-vinylcyclopropanecarboxaldehyde, changing the concerted mechanism into a stepwise one (*J. Phys. Chem. Lett.* 2019, **10**, 2991–2997). However, as a proof-of-concept, we have demonstrated that electrostatic effects have significant impacts on fragmentation reaction barriers. These conclusions lead to interesting questions on the effect of EEFs and more generally, local electrostatic environment, on dynamic effects such as dynamic matching and PTSBs. Work in our group is currently being carried out to answer these questions.

